Light Scattering: Quasi-elastic Rayleigh Scattering Spectroscopy

Max Christopher* and Xiaoyuan Zhang†
Department of Physics, Harvard University, Cambridge, MA 02138

In this paper, we measured light scattering in the Rayleigh region and the coherent backscattering region. In particular, for Rayleigh scattering, we studied the relationship between the time constant and the scattering angle for samples with different particle sizes and concentrations. From these results, we calculated the corresponding diffusion constants. Also, by investigating the intensity of the coherent backscattering cones produced by solutions with different particle concentrations, we determined the transport mean-free-path of the particles in the solution. From this value, we were able to reaffirm the solution's concentration.

I. INTRODUCTION

1 Particles suspended in an aqueous solution undergo Brownian motion which is simply random motion determined by their own collisions. When presented with a concentration gradient, these particles will diffuse from a high concentration to a lower one, attempting to reach an equilibrium. When light is passed through a solution of these particles undergoing this random motion, the light is scattered. This means that the light is deflected off of the particles in the solution which changes its direction. However, the way in which the light is scattered, is dependent on both particle size and solution concentration. In this paper we investigate two primary regimes of light scattering: Rayleigh scattering and coherent backscattering.

A. Diffusion & Rayleigh Scattering

2 If the sizes of the scattering particles are smaller than the wavelength of the light, then Rayleigh scattering [1–5] will model the scattering effect. Rayleigh scattering leads to various phenomena in nature. For example, it explains why the shorter wavelengths of the visible light spectra are scattered more in the atmosphere, making the sky blue. Unfortunately, the Rayleigh scattering model begins to break down as the size of the scattering particles increases, specifically, as the particles become within an order of magnitude of the scattering light. This scattering must be modeled with Mie theory [6], however we will not go into Mie scattering in this paper.

3 It has been observed that the diffusive motion of particles can be characterized by studying the light scattering effects within the Rayleigh region [7–10]. Consider the probability $P(\vec{r},t|0,0)d^3r$ that a particle at $(\vec{r}=0,t=0)$ is scattered to the position $(\vec{r},t)$. If the particle is described by Brownian motion, the form of this probability is simply [11, 12]

$$P(\vec{r},t|0,0) = (\pi D t)^{-3/2} \exp\left(-\frac{r^2}{4Dt}\right) \tag{1}$$

where D is the diffusion constant. The diffusion coefficient has units of area over time and represents the rate at which a particular substance diffuses across a gradient. Specifically, the diffusion coefficient is the amount of a particular substance that crosses a unit area in one second under the influence of a unit gradient [13]. Ultimately, this coefficient characterizes the diffusion of the solution in the stationary phase. Generally, the evolution of this probability can be updated by performing a three-dimensional random walk. However, if the particle is a sphere with the radius a, the Stokes-Einstein relation [14] implies that

$$D = \frac{k_B T}{6\pi\eta a} \tag{2}$$

where k_B is the Boltzmann constant, T is the temperature and η is the viscosity of the solvent.

4 With the addition of the dipole approximation, we can calculate the average light scattering spectrum. Given wave numbers $\vec{k}_i$ and frequencies ω_i, with the incident light beam described with $\vec{E}_0 e^{i(\vec{k}_0\cdot\vec{r}-\omega_0 t)}$, the total electric field $\vec{E}(t)$ induced by the particles in the solution can be measured by a detector at the distance $\vec{R}$, such that

$$\vec{E}(t) = \sum_{i=1}^{N} \vec{E}_j(t) = \sum_{i=1}^{N} \vec{E}_0' e^{i(\phi_i(t)-\omega_0 t)} \tag{3}$$

where i runs over all N particles. From classical electromagnetism, one can determine the average amplitude $\vec{E}_0'$ and the phase $\phi_i(t)$ [8]. In particular, the phase factor is the difference of the path length between the particle j and the origin (see Fig. 1). Thus we have that

$$\phi_j(t) = (\vec{k}_0 - \vec{k}_s)\cdot\vec{r}_j(t) \equiv \vec{K}\cdot r_j(t) \tag{4}$$

while the scattering vector $\vec{K}$ is determined by geometry:

$$K = 2k_0 \sin\frac{\theta}{2} = \frac{4\pi n}{\lambda}\sin\frac{\theta}{2} \tag{5}$$

Here the scattering angle, θ, is defined as the angle between $\vec{k}_0$ and $\vec{k}_s$, and n is the index of refraction of the solution.

5 Ultimately, the diffusion constant, D, can be determined from the analysis of the frequency of the light at

* maxwellchristopher@college.harvard.edu
† xiaoyuanzhang@g.harvard.edu

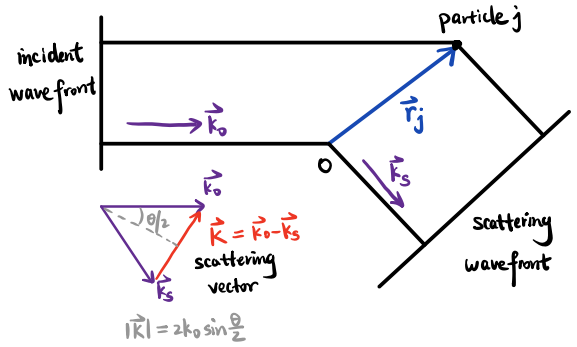

FIG. 1. A particle in the solution scattered by the light. The scattering vector K is computed in the triangle formed by $\vec{k}_0$ and $\vec{k}_s$.

different scattering angles. The intensity of the scattered light is written as $I(t) \sim |E(t)|^2$. For our experiment, we will need to consider the average intensity $\langle I(t)\rangle$ and the autocorrelation function $C(t') = \langle I(t)I(t+t')\rangle$. Clark, Lunacek, and Benede show in Ref. [8] that the theoretical prediction of the autocorrelation function gives

$$C(t') = N^2|E_0'|^4\beta^2\left(1 + e^{-2DK^2t'}\right) \tag{6}$$

where $\beta = cn\epsilon_0/2$. Using Wiener-Khinchin Theorem [15–18], one can perform the Fourier transform of $C(t')$ and obtain the power spectrum as a function of frequency, $S(\omega)$ such that

$$S(\omega) = N^2|E_0'|^4\beta^2\left(2\pi\delta(\omega) + \frac{4DK^2}{\omega^2 + (2DK^2)^2}\right) \tag{7}$$

The half-width of this curve, γ, is inversely proportional to the mean decay time τ such that:

$$\gamma = \frac{(\Delta\omega)_{1/2}}{2\pi} = \frac{1}{2\pi\tau} \tag{8}$$

The diffusion coefficient is obtained from the half-width of the spectrum, giving us the relation

$$\frac{1}{\tau} = 2DK^2 = 2D\left(\frac{4\pi n}{\lambda}\right)^2 \sin^2\frac{\theta}{2}. \tag{9}$$

Thus, we have found a relation for D dependent upon K, the scattering vector from Eq. (5) and the frequency of the scattered light.

B. Coherent Backscattering

6 There is another interesting form of light scattering called the coherent backscattering (CBS) of light. Consider a beam of light that is aimed at a solution of particles in Brownian motion. The incident photons deflect off particles in the solution with a transport mean-free-path length l^*, but the light also interferes with itself as it scatters [19]. Notice that l^* is equivalent to the average distance between the particles in the solution. After multiple deflections, some photons will exit the solution in the opposite direction as the incident light. These photons that are traveling the same path as the incident light, but in the opposite direction, are called the time-reversed mates of the incident photons. These time-reversed paths then constructively interfere in the opposite direction as the incoming light [19] as we will show below.

7 Using the geometry of some scattering path and a time-reversed path, we can show that the difference in the phases of the light, $\Delta\phi$, is determined by

$$\Delta\phi = \frac{2\pi}{\lambda}\theta R \tag{10}$$

where θ is the scattering angle relative to the backscattering direction, and R is the distance between the first and last scattering particle. The mean-square value of R is dependent upon the diffusion coefficient, D, which can itself be written in terms of the speed of light, c, and l^* such that

$$\langle R^2\rangle = 6Dt = 6\frac{cl^*}{3}t. \tag{11}$$

Here, t is the random walk time, which means that we can write the total scattering path length, s, as $s = ct$. Using the root-mean square-value of R to determine the phase difference, we find that

$$\Delta\phi = \frac{2\pi}{\lambda}\theta\sqrt{2l^*s} \tag{12}$$

However, in order to constructively interfere, the phase difference must be very small. This means that $\Delta\phi/(2\pi)$ must be much less than 1. Therefore, there is some critical angle such that

$$\theta_c = \frac{\lambda}{\sqrt{2l^*s}} \tag{13}$$

This shows that light backscattered within this critical angle will create a clear intensity cone as the light constructively interferes with itself. Importantly, note that the maximum cone width results from the smallest path length s. The smallest average path length is the distance between two particles, $s = l^*$. This shows that the maximum angular cone width is given by

$$\theta_{\max} = \frac{\lambda}{\sqrt{2}l^*} \tag{14}$$

Thus, the width of the CBS cone, $\theta_{\max} = 2\gamma$ (recall that γ is the half-width of the cone's peak), is inversely proportional to the transport mean-free-path length [19].

C. Experiment Motivation

8 In this experiment we will investigate multiple properties of systems in Brownian motion associated with

their light scattering effects. By using a laser beam incident on a solution of particles of a controlled size, and recording the light at different scattering angles, we will determine the solution's diffusion coefficient using the Rayleigh scattering model. We will also observe the CBS intensity cone within the backscattering regime. By analyzing the intensity, we will determine the transport mean-free-path lengths of the solution and their concentrations.

9 These experiments show that we can obtain lots of data about a solution based on only its scattered light. These scattering effects encode information about the solutions they pass through and allow us to uncover them indirectly. This could carry huge implications for remote sensing and data collection where direct sampling of a solution is impossible. Ultimately, the effects of light scattering are extremely important to understand for these and potentially other unique benefits.

II. RAYLEIGH SCATTERING EXPERIMENT

A. Rayleigh Scattering Apparatus

10 In order to investigate the properties associated with Rayleigh scattering we used a 20 mW Nd-YAG laser with a wavelength of 532nm. First, we aligned the laser so that it was parallel to the table using a matrix of four mirrors (see the process in Appendix 1). With the straight laser beam, we aligned the optics as shown in Fig. 2. We first focused the laser onto the sample using a 100mm lens. The sample was placed at the axis of a rotating plate holding the rest of the optics. The laser beam then passed through an aperture to restrict the solid angle the beam would cover. Finally, the beam was focused on the detector using a 75mm lens followed by a 55mm lens creating a telescopic effect with the focused light. By measuring the angle of the rotating plate with respect to the optics table, we can determine the scattering angle that the detector is measuring. The signal from the detector is then passed to a transimpedance amplifier and recorded on the fast Fourier transform (FFT) program on the computer. The FFT program allows us to save the incoming signal data as a power spectrum dependent on frequency.

B. Rayleigh Methods

11 We began the Rayleigh scattering experiment by preparing three microsphere solution samples for analysis by the procedure outlined in Appendix 2. We created a 5:1000 and 4:1000 concentration of 0.063 μm microspheres and a 1:1000 concentration of 0.50 μm microspheres. With the sample placed in the apparatus described in Section II A, we began to collect data for different scattering angles. We found that the ideal gain for the detector was at a gain of 20. Using the

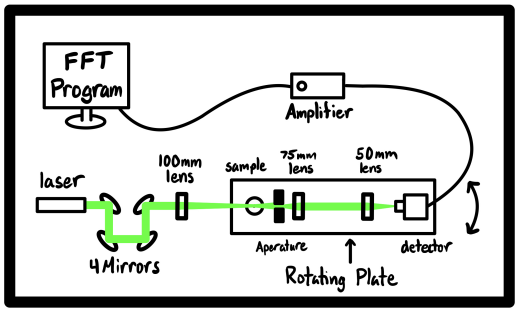

FIG. 2. A diagram of the Rayleigh scattering apparatus. Notice that the rotating plate has an axis of rotation about the sample. Thus, as the tray rotates, the detector can record the signal at different scattering angles.

LabVIEW light scattering FFT program, we took 4096 samples at a sample rate of 2048 samples per second. The LabVIEW program records the incoming signal as a voltage with respect to time and automatically performs the Fourier transformation converting the measurements into the power spectrum. As each measurement only took 2 seconds, we compiled 50 data sets per angle in order to reduce statistical error. We recorded the power spectra of angles at 2.5 degree intervals starting from 0 degrees being parallel to the incident beam. We were able to drastically limit the background noise picked up by the detector, but despite its minimal amplitude, we still subtracted this value from the final data sets.

12 With the background subtracted, we calculated the average power spectrum for each angle with an error determined by the standard deviation. According to Clark, Lunacek, and Benedek [8], the leading term in the power spectrum is a single Lorentzian distribution centered about zero (see Eq. 20 in Appendix 3 b). The half-width, γ, of the fitting is related to the time constant τ in the autocorrelation function: $\gamma = 1/(2\pi\tau)$ from Eq. (8). Calculating the time constant τ for each angle, we can verify Eq. (9) and determine the diffusion constant D. We will also propagate the error from the measurement to the diffusion constant D. Repeating the analysis for all samples, we can investigate the dependence of the diffusion constant on the size of the particles in the solution.

C. The Results of Rayleigh Scattering

13 Fig. 3 shows the power spectra for two different solutions of different particle size and concentration at multiple scattering angles. It is clear from both samples that the power of the scattering increases with smaller angles and lower frequencies. While the 0.063 μm microsphere solution falls into the Rayleigh region, the 0.500 μm microsphere solution is approaching the Mie scattering region as we are using a 532nm laser. However, since there is no strict boundary between these two region, we will

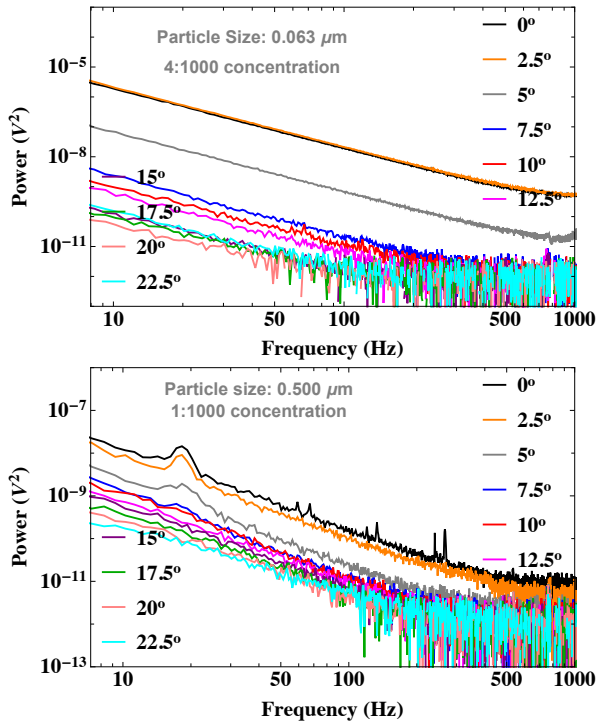

FIG. 3. The average power spectrum for light scattering at different scattering angles, with the 4:1000 concentration of 0.063 μm microspheres and and the 1:1000 concentration of 0.500 μm microspheres respectively. Here, the error is estimated by repeating 50 measurements. Note that we join the experimental points into lines in order to distinguish different angles.

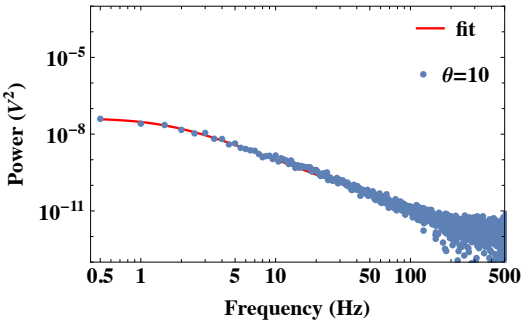

FIG. 4. The numerical fitting for the power spectrum using the 0.500 μm case at $\theta = 10$ degrees as an example.

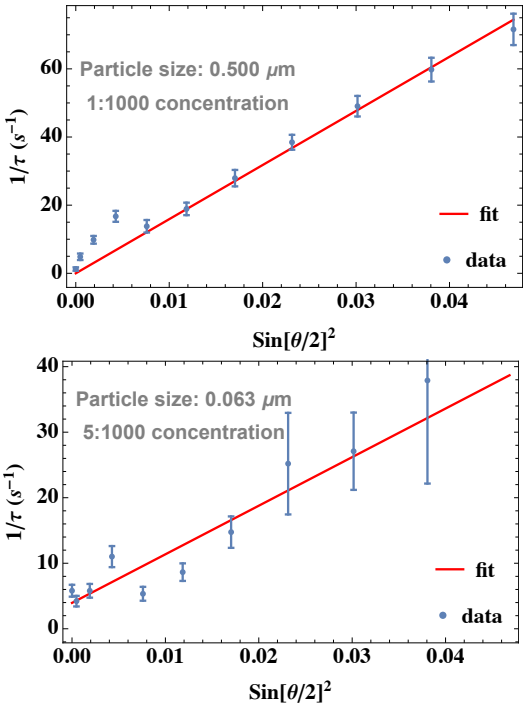

FIG. 5. The relationship between the time constant and the scattering angle. The large particle size exhibits better linear fitting despite deviation in extremely small angles, while a linear model does not appear to be a good fit for the smaller size.

analyze the larger case using the dipole approximation in this experiment.

14 We found that the intensity decreases as we increase the scattering angle. To study this relation quantitatively, we fit the spectrum with a Lorentzian distribution [20, 21] centered about the origin, but also had to add a constant to characterizes the background. Fig. 4 shows one example of this numerical fitting. Using Eq. 20, we can obtain the half-width directly from the fit parameters, which we can then use to determine the time constant τ. Table I gives the time constant for all angles in the 0.500 μm microsphere solution. Using these values for τ, we found that the 0.500 μm microsphere solution scattered in agreement with Eq. (9), as shown in Fig. 5.

15 We found that the concentration of the solution affects the overall intensity of the scattered light. Comparing Fig. 6 and the 0.063μm sample from Fig. 3, we see that the intensity decreases as we increase the concentration for a fixed angle and fixed frequency. This makes sense because the amount of light that passes through the solution decreases with increasing solution density. With respect to the particle sizes, we expect less diffusion and light scattering as the microspheres increase in size. However, we were unable to get a good fit for the small size data sample and thus have no way to calculate the diffusion coefficient precisely (see Fig. 5). Assuming the index of refraction for the solution is the same as water, we obtain $D = 1.54 \pm 0.45$ μm^2/s for 0.500 μm size and $D = 1.10 \pm 0.40$ μm^2/s for 0.063 μm size using Eq. (5).

16 There are two potential problems in our data for Rayleigh scattering. First of all, there might exist some low frequency noise in our spectrum, causing a large deviation from the correct Lorentzian distribution. Also, there could be unwanted light entering the detector at specific angles, which comes from the reflection off of certain optics. Additional information about Rayleigh

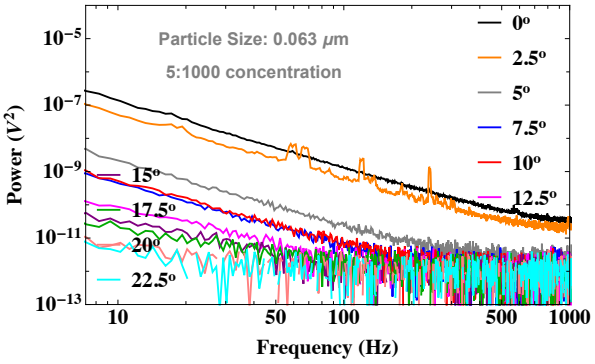

FIG. 6. Average power spectrum for light scattering at different scattering angles, with 5:1000 concentration of 0.063 μm microspheres. We see that the intensity is lower with this higher concentration.

scattering and the error in our data can be found in Appendix 4.

17 In the above analysis, we have not accounted for the effects of the aperture. As shown Fig. 2, the width of the light beam is controlled by the aperture. Therefore, when we fix the detector at some angle θ, we are actually measuring the light within the solid angle $\theta \pm \delta\theta$, where $\delta\theta$ is determined by the diameter of the aperture. In our experiment, the diameter was $d = (1.01 \pm 0.02)$ mm and the distance from the sample to the aperture is $L = (28.27 \pm 0.18)$ mm. This means that we can calculate $\delta\theta = 2\tan^{-1}\left(\frac{d}{2L}\right) = (0.0356 \pm 0.0008)$ rad. The angle associated with this solid angle is thus much less than the systematic error associated with measuring the angle of the rotating plate by hand. Therefore, we consider the effects of this $\delta\theta$ to be negligible.

Angle (Degrees)	0	2.5	5	7.5	10	12.5
τ	1.25 ± 0.51	4.85 ± 0.95	9.83 ± 1.13	16.72 ± 1.61	13.80 ± 1.84	18.90 ± 1.84
Angle (Degrees)	15	17.5	20	22.5	25	
τ	27.93 ± 2.41	38.46 ± 2.19	49.05 ± 3.01	59.78 ± 3.48	71.59 ± 4.60	

TABLE I. A table of the scattering angles and the experimentally determined τ values for the 0.500 μm microsphere solution.

III. COHERENT BACKSCATTERING EXPERIMENT

A. Backscattering Apparatus

18 To evaluate the CBS cone, we needed to set up a different optical apparatus as shown in Fig. 7. For this experiment we used the same 532nm laser as in the Rayleigh scattering apparatus with four equivalent alignment mirrors. Next, the light passes through a beam expander, which is a 100mm lens followed by a 400mm lens. The beam then travels through a periscope, because our entire apparatus spanned two separate optical tables and we were forced to lower the beam. Next, a mirror reflects the beam into a 50/50 beam splitter. Half the beam goes to a beam stop while the other half is directed through a quarter wave plate to give the light a circular polarization. Here the light encounters the sample and the light is scattered. The directly backscattered light travels back through the quarter wave plate, and re-enters the beam splitter. Half the light follows the path back to the laser, but the other half is sent into a 500mm focusing lens followed by an adjustable polarizer. Because the laser had an initial polarization in the vertical direction, we experimentally determined that this polarizer had to be adjusted to be vertical with respect to the table to observe the backscattering cone. Finally, the light is detected by the Hamamatsu photomultiplier

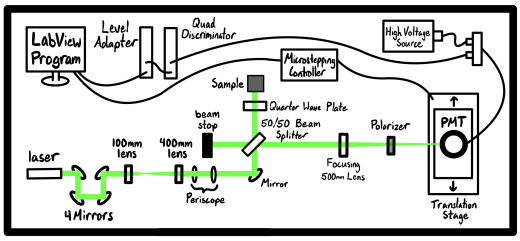

FIG. 7. A diagram of the coherent backscattering apparatus. Note that the light backscattered from the sample is not a perfect beam as shown above. This is depicted as such for conceptual understanding, but the light is actually spread widely with a cone of more intense light in the direct backscattering direction.

tube (PMT). This PMT detector is mounted on a motorized translation stage that is controlled by the computer. This allowed us to take measurements at extremely precise position intervals. The PMT is connected to the high voltage for power. Its signal is passed through a quad discriminator which establishes a threshold of 100mV, eliminating some of the reflected signals along the cable. It also converts the signal to a logic pulse to be read by the computer. Finally, the signal was made positive by the level adapter before it was displayed on the `LabVIEW` program.

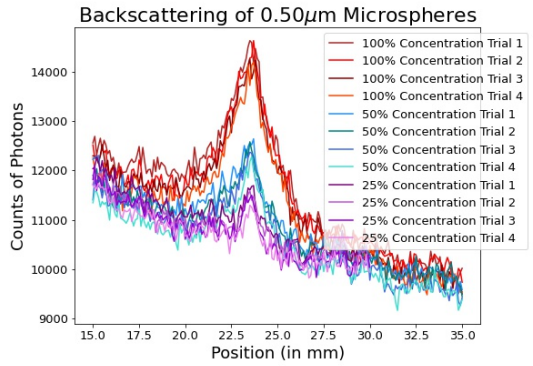

FIG. 8. This figure displays the four data sets collected for each microsphere concentration. This diagram clearly shows the correlation between decreasing concentration and decreasing intensity of the CBS cone.

B. Backscattering Methods

19 We prepared three microsphere concentrations to test for our backscattering experiment. To be able to observe the CBS cone, we needed to use a high concentration of microspheres, so we used 100%, 50% and 25% microsphere concentrations. Appendix 5 explains why these microsphere solutions refer to the concentration of the out-of-container solution and not the percentage of microspheres to water. We used these three samples to collect backscattering data with the described apparatus.

20 We collected four data sets per concentration, recording photon counts at each position, taking measurements at 0.100 mm intervals on the translation stage. We used `Python` to compile the data and each data set contained a clear CBS peak as seen in Fig. 8. Next, we calculated an average and a standard error of the mean for each concentration. Before we fit the data, we converted the position of the translation stage to the backscattering angle in radians (see Appendix 6). With this conversion complete, we could fit the three averaged CBS cones with a linear plus lorentzian (Eq. 21) function using `Python`'s curvefit, while taking the error into account. This can be seen in Fig. 9.

C. The Results of Backscattering

21 Importantly, the linear plus lorentzian curve fitting gave us a value for the half-width (γ). From here, it is simple to calculate the full-width at half maximum (2γ), which is simply twice the half-width. The full-width is also represented by $\theta_{\max}$ from Eq. 14. Therefore, we can use 2γ and the wavelength of our laser (which is 0.532μm) to calculate the theoretical transport mean-free-path length, l^*, of each sample. These results are displayed in Table II.

Sample	Half-Width (γ)	Full-Width at Half Max (2γ)	Transport Mean-Free-Path Length (l^*)
100%	$1.26 \cdot 10^{-3} \pm 2.310 \cdot 10^{-5}$	$2.52 \cdot 10^{-3} \pm 4.619 \cdot 10^{-5}$	149 ± 2.737 μm
50%	$8.08 \cdot 10^{-4} \pm 2.495 \cdot 10^{-5}$	$1.62 \cdot 10^{-3} \pm 4.990 \cdot 10^{-5}$	232 ± 7.160 μm
25%	$3.18 \cdot 10^{-4} \pm 2.393 \cdot 10^{-5}$	$0.64 \cdot 10^{-3} \pm 4.786 \cdot 10^{-5}$	591 ± 44.203 μm

TABLE II. Here, we show the half and full-widths determined by our linear plus Lorentzian curve-fitting measured in radians for all three backscattering samples. We also display their experimentally determined values of transport mean-free-path length.

22 As shown in Appendix 5, our order-of-magnitude approximation for an expected l^* value was $l^* = 500\mu$m. Unfortunately, due to the conditions of our original sample, this order-of-magnitude approximation is the best we can do to evaluate the validity of our results. However, this approximation does support our predicted l^* values as shown in in Table II. In fact, these results would lead us to believe that our reconstituted microsphere solution had a concentration of microspheres greater than 10% by volume (for the 100% sample), as they were packed together tighter than our 450μm approximation. Using the same crystal lattice approximation as outlined in Appendix 5, we can approximate the solutions' actual concentration using Eq. 22, solved for the concentration. This gives us that the concentration p of microspheres in the solution is

$$p = \frac{50}{l^* + 50} \tag{15}$$

The precise concentrations determined by l^* are shown in Table III.

Sample	l^*	Concentration
100%	149 ± 2.737 μm	$25.13 \pm 0.00346\%$
50%	232 ± 7.160 μm	$17.73 \pm 0.00450\%$
25%	591 ± 44.203 μm	$7.80 \pm 0.00540\%$

TABLE III. The experimentally determined concentrations determined by Eq. 15 for each of the three samples.

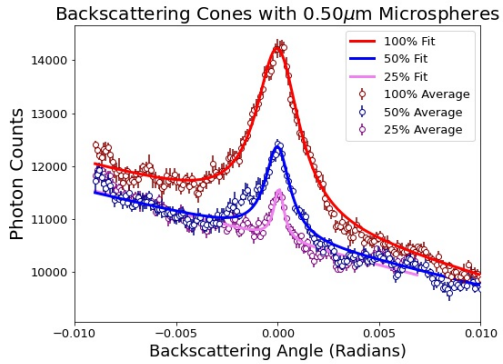

FIG. 9. This figure shows the averaged data set for each concentration along with their associated error. Each concentration is fit with a linear plus lorentzian function.

Therefore, the backscattering cone allowed us to determine l^* and to approximate the reconstituted concentrations of the microspheres.

23 It appears that our sample concentrations disagree with our experimentally determined concentrations of microspheres from the CBS cones. Specifically, 17.73 is not 50% of 25.13, while 7.80 is close to 25% of 25.13. This error could have come from a few factors. Primarily, this discrepancy can be accounted for in the creation of the samples. As described in Appendix 5, the reconstituted solution was fairly imprecise and may not have been evenly distributed within the solution. Furthermore, microspheres would get stuck inside the pipette while creating samples which could have made slight variations in the diluted samples. Other errors could have certainly been reduced if we had the time to take more than just four data sets per concentration.

IV. CONCLUSION

24 In this paper, we present the measurements of Rayleigh scattering and coherent backscattering. For Rayleigh experiments, we measured the intensity of light scattered by samples with different particle sizes at different scattering angles. For each sample, we verified the relation in Eq. (9) and calculated the corresponding diffusion coefficients D. For the coherent backscattering experiment, we evaluated solutions of different particle concentrations. We showed that by measuring the width of the backscattering cones, we were able to determine the l^* value of the solution. This was an informative property of the solution which then allowed us to approximate the solution's concentration.

V. ACKNOWLEDGEMENTS

We thank Matteo Mitrano for the help with the alignment of Rayleigh scattering and data analysis in both experiments. We also appreciate Joe Peidle and Jieping Fang for teaching us how to use the equipment, design the experiment, and in particular, analyze the problem of Rayleigh scattering data. Moreover we thank Jenny Hoffman for enlightening discussions and useful suggestions on the manuscript.

In order to divide the work for this report, Xiaoyuan was primarily responsible for the background and data analysis of the Rayleigh scattering while Max completed the same for the backscattering. That being said, this was a collaborative effort and we assisted each other with all elements of the report.

[1] J. W. Strutt, Xv. on the light from the sky, its polarization and colour, The London, Edinburgh, and Dublin Philosophical Magazine and Journal of Science **41**, 107 (1871).
[2] J. Strutt, Xxxvi. on the light from the sky, its polarization and colour, The London, Edinburgh, and Dublin Philosophical Magazine and Journal of Science **41**, 274 (1871).
[3] J. W. Strutt, Lviii. on the scattering of light by small particles, The London, Edinburgh, and Dublin Philosophical Magazine and Journal of Science **41**, 447 (1871).
[4] L. Rayleigh, X. on the electromagnetic theory of light, The London, Edinburgh, and Dublin Philosophical Magazine and Journal of Science **12**, 81 (1881).
[5] L. Rayleigh, Xxxiv. on the transmission of light through an atmosphere containing small particles in suspension, and on the origin of the blue of the sky, The London, Edinburgh, and Dublin Philosophical Magazine and Journal of Science **47**, 375 (1899).
[6] G. Mie, Beiträge zur optik trüber medien, speziell kolloidaler metallösungen, Annalen der physik **330**, 377 (1908).
[7] J. C. Brown, Optical correlations and spectra, American Journal of Physics **51**, 1008 (1983).
[8] N. A. Clark, J. H. Lunacek, and G. B. Benedek, A Study of Brownian Motion Using Light Scattering, American Journal of Physics **38**, 575 (1970).
[9] R. Pecora, Doppler Shifts in Light Scattering from Pure Liquids and Polymer Solutions, J. Chem. Phys. **40**, 1604 (1964).
[10] H. Z. Cummins, N. Knable, and Y. Yeh, Observation of Diffusion Broadening of Rayleigh Scattered Light, Phys. Rev. Lett. **12**, 150 (1964).
[11] C. Kittel, *Elementary Statistical Physics*, Dover Books on Physics (Dover Publications, 2012).
[12] M. C. Wang and G. E. Uhlenbeck, On the Theory of the Brownian Motion II, Reviews of Modern Physics **17**, 323 (1945).
[13] L. S. Ettre, Development of chromatography, Analytical Chemistry **43**, 20A (1971), pMID: 22716676, https://doi.org/10.1021/ac60308a022.

[14] A. Einstein, *Investigations on the Theory of the Brownian Movement*, Dover Books on Physics Series (Dover Publications, 1956).
[15] N. Wiener, Generalized harmonic analysis, Acta Mathematica **55**, 117 (1930).
[16] D. Champeney, Power spectra and wiener's theorems, A Handbook of Fourier Theorems , 102 (1987).
[17] A. Khintchine, Korrelationstheorie der stationären stochastischen prozesse, Mathematische Annalen **109**, 604 (1934).
[18] A. Einstein, Méthode pour la détermination de valeurs statistiques d'observations concernant des grandeurs soumises à des fluctuations irrégulières, Archives des Sciences **37**, 254 (1914).
[19] R. Corey, M. Kissner, and P. Saulnier, Coherent backscattering of light, American journal of physics **63**, 560 (1995).
[20] N. Johnson, S. Kotz, and N. Balakrishnan, *Continuous Univariate Distributions*, Continuous Univariate Distributions No. v. 2 (Wiley & Sons, 1994).
[21] W. Feller, V. Feller, and K. M. R. Collection, *An Introduction to Probability Theory and Its Applications*, An Introduction to Probability Theory and Its Applications No. v. 1-2 (Wiley, 1957).
[22] W. B. Davenport, W. L. Root, *et al.*, *An introduction to the theory of random signals and noise*, Vol. 159 (McGraw-Hill New York, 1958).
[23] F. Reif, *Fundamentals of Statistical and Thermal Physics* (Waveland Press, 2009).

APPENDIX

1. Laser Alignment

25 In order to ensure the laser was parallel to our experiment table, we completed a four mirror alignment. First we used a combination of two mirrors to ensure that the beam was parallel to the table. To do so, we ensured that the output beam passed through two apertures of identical height. Next, we used two more mirrors to ensure that the light was also parallel with the instrument bolts on our experiment table. We completed this in a similar manner, making micro-adjustments on the two mirrors until the beam passed through two apertures of identical height on the plane of pour experiment.

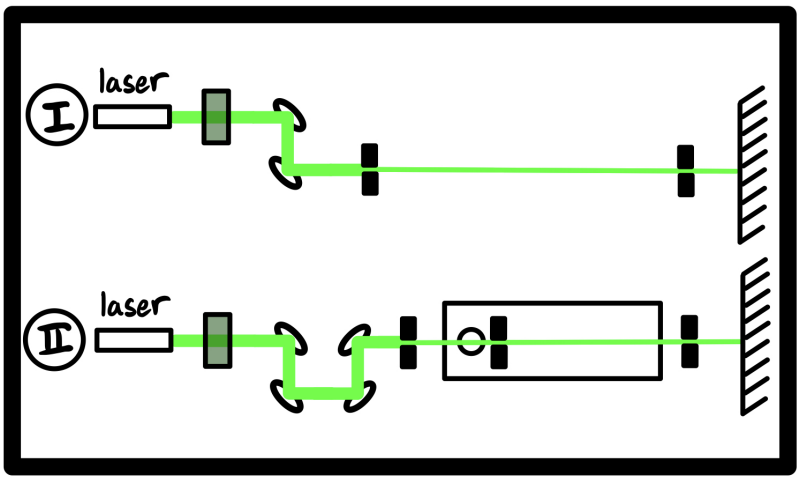

FIG. 10. (I) Shows the first step of the alignment procedure making the beam parallel to the table and (II) aligns the beam along our experiment.

2. Preparing Samples

26 We had to create microsphere solutions with a precise ratio of microspheres to distilled water in order to study the effects of scattering. After selecting the applicable diameter of microspheres, we had to mix the container using the MaxiMix device from the lab. Then, to create our precise ratio, we would pipette N microliters (μL) of the microspheres and X milliliters (mL) of distilled water into a glass test tube. This would give us a solution with a concentration of $N : X \times 10^3$ microspheres to distilled water. Then we covered the glass test tube with a thin paraffin seal, and mixed and suspended the solution with the MaxiMix. Finally we cleaned the glass to prepare it for measurement.

3. Mathematics Background

a. *Wiener-Khinchin Theorem*

27 Consider a field $E(t)$ and its autocorrelation function $C(t)$

$$C(t) = \int_{-\infty}^{\infty} E(\tau)^* E(t+\tau) d\tau \tag{16}$$

Since the Fourier transformation of the field is

$$E(\tau) = \int_{-\infty}^{\infty} E(\omega) e^{-i\omega\tau} d\omega$$

$$E^*(\tau) = \int_{-\infty}^{\infty} E^*(\omega) e^{i\omega\tau} d\omega \tag{17}$$

it is straightforward to calculate the autocorrelation function

$$C(t) = \int d\tau d\omega d\omega' E(\omega) E^*(\omega') e^{-i\omega\tau} e^{i\omega'(\tau+t)} = \int_{-\infty}^{\infty} |E(\omega)|^2 e^{-i\omega t} d\omega \tag{18}$$

Therefore, the autocorrelation is simply the Fourier transform of the squared field. This is known as Wiener-Khinchin Theorem [15–18] and it is nicely summarized in Ref. [22, 23].

28 In our experiment, the power spectrum of the Rayleigh scattering Eq. (7) can be obtained in the same way with

$$S(\omega) = \int_{-\infty}^{\infty} e^{i\omega t'} C(t') dt' \tag{19}$$

b. *Lorentzian Distribution*

29 The Lorentzian distribution [20, 21] is widely used to describe peaks in all aspects of physics. The Lorentzian distribution is written as

$$f(x; x_0, \gamma) = \frac{1}{\pi\gamma} \frac{\gamma^2}{(x_0 - x)^2 + \gamma^2} \tag{20}$$

where x_0 is the location of the peak of the distribution and γ is the half-width of the peak. For Rayleigh scattering, we used the distribution centered about the origin (with $x_0 = 0$) to fit the data for a variable frequency. For the purposes of the backscattering experiment, we needed to add a linear term to the Lorentzian function to compensate for the background. Our independent variable was the backscattering angle, θ, so it was sufficient to use the following equation:

$$f(\theta) = m\theta + A \cdot \frac{\gamma}{(x_0 - \theta)^2 + \gamma^2} + b \tag{21}$$

Here, m is the slope, b is the background and A represents the total amplitude of the curve (this parameter A incorporates the $1/\pi\gamma$ from Eq. (20)).

4. Failed trials of Rayleigh Scattering

30 In this section, we present other experiments we completed for the Rayleigh scattering. In all, we prepared four microsphere samples: two of them were 5:1000 concentrations of 0.063 μm microspheres; the third one was a 4:1000 concentration of 0.063 μm microspheres; and the final one was a 1:1000 concentration of 0.500 μm microspheres.

31 We completed the scattering measurements twice using the identical 5:1000 concentrations of 0.063 μm microspheres and obtained similar average power spectra (see Fig. 6 and Fig. 11 respectively). In our initial data collection, we determined that the data for small particles did not behave as expected. Therefore, we decided to test this equivalent concentration and size while taking extra precautions to ensure the data was as clean as possible. We tried to use a rectangular test tube for scattering, set up additional foam core blocks to limit reflections from other optics, inflated the optical table's feet to eliminate low frequency shaking from the building and even offset the plane of the detector to improve its received light quality. While we were able to collect data at larger angles for our second measurement, none of the distributions were improved and none appeared characteristically Lorentzian. In both figures, the plots look relatively linear in the log-log scale, while we expected a plateau at low frequencies followed by a steep drop off. One problem comes from this low frequency region, as it is too high compared with the standard result. It is possible that there are some low frequency signals (other than light) entering the spectrum which are not detected during the background measurement. Another issue is that when fitting the data with a Lorentzian distribution, we are not able to get stable plots. Adding a linear function (or even a quadratic function), or changing the region of the data for fitting did not improve it. Using the larger scattering angles measured in our second trial of this experiment, we were also able to obtain a diffusion constant, $D = 0.86 \pm 0.03$ μm^2/s, which is different from the one determined in Sec. II C. While the relation between the small scattering angles and τ are shown in Fig. 5, we show the larger scattering angle plot in Fig. 12.

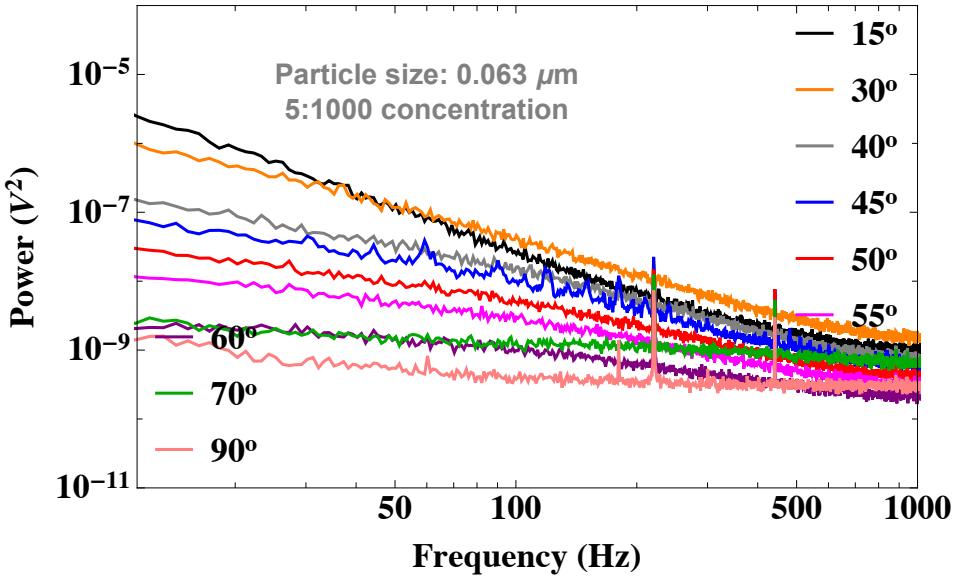

FIG. 11. A second average power spectrum for light scattering at different scattering angles, with a 5:1000 concentration of 0.063 μm microspheres. Despite many precautions to limit background light and other error, note the similar plot structure to the equivalent measurements in Fig. 6.

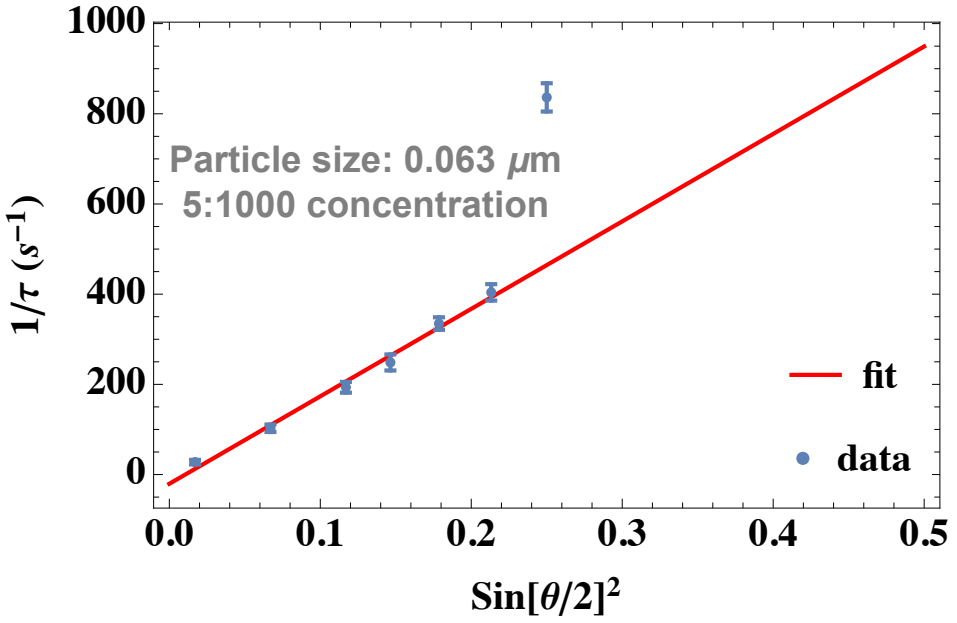

FIG. 12. The relation between the scattering angle and the time constant, with the second 5:1000 concentration of 0.063 μm microsphere solution. Note its difference from Fig. 5, as we were able to focus on the large angle region in this trial.

32 For the third sample of the 4:1000 concentration of 0.063 μm microspheres, we got even worse data for the time constant. For some angles, the half-width was around $10^{-5}/s^{-1}$ due to the bad fitting. Therefore, we only used this concentration to show the difference of the intensity.

33 The large particle size had the best result, as shown in Fig. 3. However, we were only able to measure the power spectra for small angle region. Despite some deviations in the extremely small angles, we observe a relatively good linear fit in Fig. 5.

5. 0.50μm Microsphere Solution Reconstitution

34 The out-of-container concentration of 0.50 μm microspheres was listed to be 10% microspheres by weight. However, when we obtained the solution from the fridge, it was completely dried out. Therefore, we had to reconstitute the microsphere solution by adding additional water and mixing for a long period of time. This left the actual concentration of the solution fairly imprecise. While solution concentrations have no effect on Rayleigh scattering, this was important information for the backscattering measurements. Therefore, we were working under the assumption that the reconstituted solution was roughly equivalent to the 10% microspheres by weight of the original solution (this was later disproved by the experimentally determined concentrations in Sec. III C). As the microspheres have a similar density to water, we can also assume that the solution was about 10% microspheres volume. This reconstituted solution is what we refer to as our 100% microsphere solution.

35 In order to estimate the approximate transport mean-free-path length (l^*) of our solution, we needed to know the precise concentration of the microspheres in our solution. This was impossible to do with the reconstituted solution, so we completed the following to find an approximation of our expected l^*: Assuming a crystal lattice, and given a 10% microsphere concentration by volume, we can find that the linear density of microspheres is also 10% when parallel to the lattice. Given some distance parallel to the crystal lattice, 90% of that distance will be water (or total space between the microspheres). Simply divide this distance by the number of 0.50μm microspheres that fit along the other 10% of this distance and we find an approximation of the mean distance between each microsphere. For example, using a sufficiently large linear distance D, we have

$$\frac{D(1-p)}{Dp/50} = \frac{50(1-p)}{p} = l^*\mu\text{m} \tag{22}$$

where p is the concentration of microspheres. Essentially, this formula just divides the total free space by the number of microspheres. For $p = 10\%$, we have

$$\frac{50(1-0.1)}{0.1} = 450\mu\text{m} \tag{23}$$

This is the transport mean-free-path length $l^* = 450\mu$m. Thus, to a good approximation, we would expect all our solutions to have an l^* value to this order of magnitude.

6. Backscattering Angle Conversion

36 We needed to convert the position of the translation stage to the backscattering angle in radians. To do so, we first measured how far the light had to travel to get from the sample to the PMT. This distance was 946mm. Next we centered the curves at the peak position of each averaged data set. This was 23.5mm for every curve. Finally to convert the translation stage position in millimeters to the backscattering angle we had to compute:

$$\theta = \tan^{-1}\left(\frac{x-23.5}{946}\right) \tag{24}$$

This equation gives us the value θ which represents the backscattering angle of the CBS cone in radians.